Journal of Hydrogeology and Hydrologic Engineering

Research Article A SCITECHNOL JOURNAL

Evaluating Three Conventional Electrode Arrays in 2d Electrical Resistivity Imaging Surveys for Studying the Sedimentary Layers and the Hydrogeological Situation in Southern Iraq

Ahmed Abdulameer[1,2,3*], Jassim M Thabit [2], Firas H AL-Menshed [3] and Broder Merkel [1]

[1]Institute for Geology, TU Bergakademie Freiberg, Gustav-Zeuner-Str. 12, Freiberg, Germany

[2]Department of Geology, College of Science, University of Baghdad, Baghdad, Iraq

[3]General Commission for Groundwater, Baghdad, Iraq

[*]Corresponding author: Ahmed Abdulameer, Institute for Geology, TU Bergakademie Freiberg, Gustav-Zeuner-Str. 12, 09599 Freiberg, Germany, Tel: 00491798871266; E-mail: ahmedarasool12@yahoo.com

Received date: January 05, 2021; **Accepted date:** January 20, 2021; **Published date:** January 27, 2021

Abstract

This study compares three conventional electrode arrays in 2D electrical resistivity imaging surveys by applying them to study the sedimentary layers and the hydrological situation in three coastal locations close to the Khor Al-Zubair, southern Iraq. At each location, a 2D imaging line of 1200 m length was implemented columnar the Khor Channel, using Dipole-dipole, Wenner and Wenner-Schlumberger arrays at the same line. The inverse models revealed the presence of three major resistivity layers, the uppermost layer has a medium resistivity attributed to the upper aquifer and is affected by the saline groundwater. The second electrical layer represents the upper aquifer, completely filled with brackish groundwater. The third, very low resistivity layer correlates to the lower aquifer and is filled with saline groundwater. Also, a hard clay bed (aquiclude) is visible on all geophysical lines in the depth range of 20 m-28 m. Results indicate that all three electrode arrays can detect the sedimentary layers and the extension of saline groundwater but with a difference in accuracy. The Wenner-Schlumberger array revealed the best results in delineating the resistivity layers, the extension of saline groundwater in the uppermost layer of aquifer and the clayey aquiclude and shows the best horizontal and vertical resolutions. The dipole-dipole array was less accurate in determining this extension of saline groundwater and the aquiclude. The Wenner array results were unsatisfactory in delineating the aquiclude and the lower aquifer. The Wenner-Schlumberger array, as hypothesized, is efficient in determining different resistivity layers, especially in the presence of horizontal and vertical structures or high background noise, and if long survey lines are required.

Keywords: 2D imaging technique; Saline groundwater extension; Dipole-dipole array; Wenner array; Wenner-Schlumberger array

Abbreviations: Wenner (WN); Dipole-dipole (DD); Wenner-Schlumberger (WS); Pole-Pole (PP); Pole-Dipole (PD); Equatorial Dipole-Dipole (EDD); Schlumberger (SC); Root Mean Square Error (RMSE)

Introduction

Subsurface geological and environmental investigations are important tasks, which can be conducted applying different techniques. Most of this techniques, however, are complex, site specific, costly, have limited extension, and might be accompanied with some other difficulties, e.g. difficult access to some sites (riparian zone) and regulatory constraints (oil facilities). In this regard geophysical investigations, especially electrical resistivity techniques, give a moderate solution and a very cost-effective and efficient alternative. These techniques depend on the existence of considerable dissimilarities in the resistivity of subsurface geological materials that can be identified by surface voltage measurements between pairs of electrodes after injecting an electrical current through pairs of electrodes [1]. Generally, many standard electrode arrays are used for 2D imaging lines: Wenner (WN), Dipole-Dipole (DD), Wenner-Schlumberger (WS), Pole-Pole (PP), Pole-Dipole (PD), and Equatorial Dipole-Dipole (EDD) [2-12], and applying each array are site and anomaly specific. Therefore, many investigations were conducted to specify the applicability of different arrays at different sites and for different targets [13-20].

In Iraq, many geophysical investigations have been conducted for different purposes. Comparing three arrays (DD, WS, and WN) showed that the WN array is the most suitable to study shallow subsurface structures in an area in Baghdad, Iraq [21], while the WS array would be a good option if the target area was deeper. For archaeological investigation, testing the efficiency of the WN, DD, and WS arrays in Uruk archaeological site east of Al-Samawah city in Iraq showed that the DD array provides the highest vertical resolution of the targeted anomalies [22]. However, for complex sedimentary deposits, the WS array was found superior among the Schlumberger reciprocal (SR), DD, and WN arrays in providing the best pictures with the best resolution for deep layers in the northern Badra district in Iraq [23].The authors confirmed the suitability of the WS array for determining different layers in areas with long survey lines and high heterogeneity. Thabit JM and Al-Zubedi AS tested the WS, WN and DD arrays in 2D imaging surveys through synthetic models to determine which array is the most effective in realizing the vertical fracture zone and three separate cavities [24]. The results showed that the WS array is the best approach to determine vertical and horizontal structures. Also tested the DD, WS, and WN arrays in the University of Technology Camp/Iraq-Baghdad to study the subsurface features. The author found that the WS array is the most suitable array for the target area, as subsurface features and three types of soil (Silty clay, clay, and sand) could be detected [25]. Applying the 2D imaging survey using WS, DD, and PD arrays across Um El-Githoaa cavity in Western Iraq revealed that the DD array was more successful in defining the cavity than the other arrays [26].

However, one of the most important issues in Iraq is groundwater as main source of water for many local communities. However, geophysical investigations in this domain are limited so far, and it is not known which method could be applied successfully to investigate such problems. Therefore, the goal of this study was to use different

arrays in a specific area in Iraq where geological and hydrogeological questions are still without reply. To achieve this goal, the Study Area (SA) close to Khor AL-Zubair (KhZ) in south eastern part of Iraq was selected, where local people are suffering from many problems. It is worth mentioning that the KhZ Channel is low land filled with water and it is an inland extension of the sea, with a measured salinity of 44,000 mg/l. Groundwater in this area, which is considered the main source of water for the local community, is deteriorating qualitatively and quantitatively, and the reasons are not defined so far. The main aquifer in this area is reported to have high salinity, which deteriorates the natural ecosystem and causes significant socioeconomic effects [27]. Therefore, many farmers abandoned their farms in some parts. The sediments in the SA are clastic sediments, which have high resistivity causing high noise in geophysical surveys. Besides, it was planned to survey as deep as possible covering a big area by applying long survey lines. Therefore, and according to these criteria, WS array was expected to give the best results. Yet, three arrays were (DD, WN and WS) applied to compare their functionality to the same location.

Material and Methods

Site description

Figure 1 shows the geological map of the SA which is a part of the region investigated previously by [27]. The SA is flat and covered at most with Quaternary deposits (clay, sand, and pebble). Quaternary sediments are both Pleistocene and Holocene deposits. The Al-Batin Alluvial Fan (Pleistocene) represents the main part of the SA [28]. It consists of sandy gravels and gravelly sand, where sand is generally medium to coarse-grained, while gravels exist as lenses with thickness in the range of 0.1 m to 2.0 m. Sheet run-off, tidal flats, and anthropogenic deposits form the core of the Holocene deposits. The sheet run-off deposits represent a mixture of outwash and wadi deposits. The tidal flats are characterized by fine-grained sediments (silt and clay) and occasionally sand [29]. Anthropogenic deposits made of bricks, plastics, pottery fragments and other man-made artifacts have a negative impact on groundwater quality.

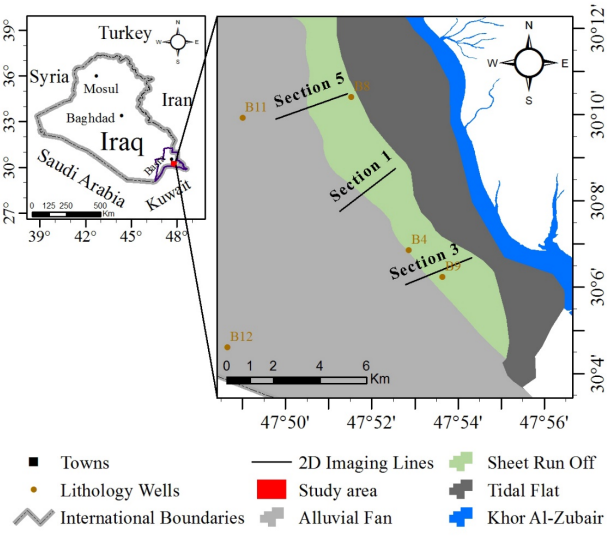

Figure 1: Left: Map of Iraq and location of the SA (red square); Right: Geological map with the main lithological units and map of the SA with locations of 2D geophysical lines (black continuous lines), Lithology bore holes (Brown circles), and KhZ (blue).

According to the Water Quality Association [30] groundwater in the SA is classified in six categories:

Fresh Water-<1,000 TDS

Brackish Water-1,000 TDS to 5,000 TDS

Highly Brackish Water-5,000 TDS to 15,000 TDS

Saline Water-15,000 TDS to 30,000 TDS

Seawater-30,000 TDS to 40,000 TDS

Brine-40,000 TDS to 300,000+TDS

The aquifer system consists of two hydrogeological units [27]: The upper unit is an unconfined aquifer and the lower unit is a confined to semi-confined aquifer of the Dibdibba Formation. A Hard Clay Bed (HCB) called "Jojab" separates these two units having a thickness in the range 2 m-4 m [31]. The saturated zone of the upper aquifer has a thickness of 15 m-20 m. It contains brackish water with TDS of 5000 mg/L-15000 mg/L [30], yet it is still to a certain degree suitable for agricultural activities. The confined to semi-confined unit located underneath contains groundwater with TDS in the range 15000 mg/L-30000 mg/L (*ibid*). Both aquifers are composed of clastic sediments [32] and groundwater table from 1 m-6 m above sea level (m.a.s.l) and it slopes to the north and north-east [33]. The groundwater flow direction is following the general topographic slope from the W and SW towards the E and NE [34]. The transmissivity of the Dibdibba aquifer is within the range of 14 m^2/day-964 m^2/day, its hydraulic conductivity is 0.38 m/d with a well discharge of 12 m^3/day-1166 m^3/day [35].

2D resistivity imaging

The survey was conducted using the SYSCAL pro$^+$ with a system of 10-channels (IRIS Instruments, Orléans, France), which is able to handle 120 electrodes. Three sites (section 1, section 3, and section 5) were chosen to apply 2D imaging profiles. It is worth mentioning here that the survey was done along these three sites two times. First, 2D imaging was applied along these sections with length of 1200 m and 10 m electrodes spacing. The survey was carried out at this step with the three aforementioned electrode arrays (DD, WN, and WS), at the same profile for each site. Second, just one array was applied along these sections with length of 2400 m and the same 10 m electrodes spacing for the purpose of detecting spatial extent of salinity contamination [27].The value of (a) for the WS and DD arrays was set to 10 m and the value of (n) was set between 1(a) and 6(a). All of these profiles have a northeast-southwest direction, columnar to the KhZ, and determine the sedimentary layers, the hydrological situation, and saline groundwater extension (Figure 1). Besides forward models nine inverse models were obtained from this survey, three models for the same profile at each site. The purpose of these nine models was to study and evaluate which electrode array can give a better 2D model for determining the sedimentary layers, the hydrological situation, and saline groundwater extension in the SA.

Four boreholes (B4, B8, B9 and B11), distributed throughout the SA (Figure 1) were used for lithological correlation and quantitative interpretation of the obtained inverse models.

The software RES2DINV ver. 3.59 (GEOTOMO SOFTWARE) was used for the purpose of data analysis and inversion. The inversion

algorithm of this software is described in details by [36-38]. The inversion method is used to estimate the true resistivity of the subsurface from field data measurements [36,37], through calculating the theoretical apparent resistivity for an inverted resistivity model of field data produced by the inversion routine. Then the Root Mean Square Error (RMSE) between the measured and calculated apparent resistivity values is determined by means of the comparison between the two pseudo sections. In the first iteration of inversion routine, the results of the forward model (apparent resistivity), which is based on an initial 2D model of resistivity distribution, is compared with actual field data; then the initial model is adjusted based on the difference. The inversion method is explained in details by [1], and the processing steps can be summarized as follows:

1 Generating apparent resistivity pseudo section from field data.
2 Generating inverse resistivity model of field data.
3 Calculating apparent resistivity pseudo section for the inverted model.
4 Comparing the two apparent resistivity pseudo sections to determine the RMS between them.
5 Modifying the inverted resistivity model according to the measured field data.
6 Generating a new calculated apparent resistivity for the inverted model.
7 Comparing the new calculated apparent resistivity model with the measured apparent resistivity one to reduce RMS between both.

Steps 1, 2, 3 and 4 represent the forward modeling, while 5, 6 and 7 represent the inversion process, and they are done in the first iteration. The iteration is repeated, decreasing the RMS until it meets a user-defined value or the number of predefined iterations is reached. Figure 2 summarized the inverse routine procedure.

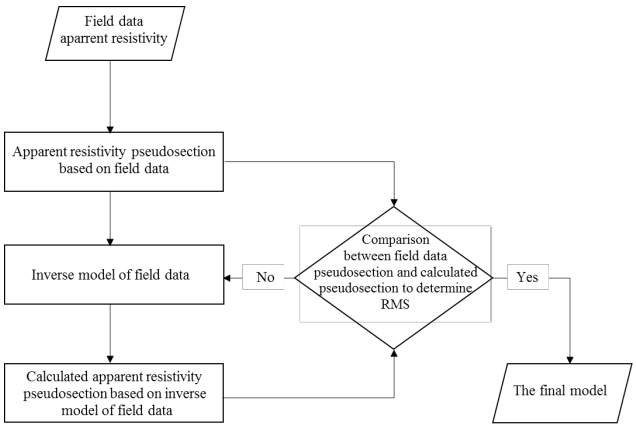

Figure 2: Flowchart of the resistivity imaging inversion.

Because of the heterogeneity near the surface and the noisy data, the initial damping factor has been set to 0.2 and the minimum damping factor has been set to 0.02. The vertical/horizontal flatness filter ratio is another critical parameter in this regard and it has been set to 0.5 due to the anomaly in the studied are extended horizontally. The standard least-squares method has been used for data inversion to minimize Root Mean Square Error (RMSE) as shown in [39]. Additionally, the RES2DINV calculates a resistivity model iteratively to minimize the difference between the calculated and observed values of apparent resistivity. The number of iterations was set to the default value 5. The obtained RMS error during the minimization of the square differences between the observed and the calculated apparent resistivity values varied between 5.0% and 10.7% over all 2D resistivity lines. Pre-processing was an important step to discard unrealistic measurements (high and low apparent resistivities) from the inversion process. For all cross sections, the bad data (excluded data) accounted for less than 6% of the total dataset.

Prefatory information about the situation in the underground was provided by previous geophysical, geochemical, hydrological and geological studies down to the investigation depth reached by the resistivity profile.A multicore 1200 m long cable and (120) electrodes were used, which is common in carrying out a 2D electrical resistivity survey. In fact, the multicore cable was divided into manageable segments, 10 m in length and connected end to end during the survey process. Furthermore, the electrodes were set into the ground at constant lengths along a survey line and linked to the multicore cable. The survey system automatically measured the apparent resistivity (ρa Ωm) in a pre-defined sequence of combinations of four electrodes.Minimizing data acquisition time was achieved by measuring several voltages simultaneously across multiple pairs of electrodes following a single impulse of electric current [1,40,41].

Sensitivity Function

One of the most important factors affecting the accuracy of resistivity measurements is the sensitivity function of the array. The sensitivity function is defined as the ability of an array to distinguish changes in the subsurface resistivity values, depending on the relative distances between the electrodes and especially potential electrodes [1]. Therefore, a high value of the sensitivity function is an indicator of the strength of the effect of subsurface materials on the measurements.Therefore, the sensitivity function can be considered as a function of clarity and accuracy as well as the investigation depth of an array [1,42]. Mathematically, the sensitivity is described by the Fréchet derivative (F) for the homogeneous hemispherical medium with limited dimensions [43]. With regard to the Depth of Investigation (DOI) it is well known in resistivity sounding surveys, that when the distance between the electrodes increases, the array can distinguish the resistivity of deeper layers.

Many authors [44-46] used a simple analytical solution (Equation 1) [2] to determine the properties of various arrays in resistivity sounding surveys [1].

$$F_{1D}(Z) = \frac{2}{\pi} \cdot \frac{Z}{(a^2+4Z^2)^{1.5}} \qquad \text{Eq. 1}$$

Z is the investigation depth and a is the spacing between electrodes, as is normal for the practical measurements of a sequence of electrode arrays. Edward LS calculated the median depth of investigation of the different electrode arrays used in one dimension resistivity sounding surveys [44]. Loke MH, Barker RD also calculated the median depth of investigation for different arrays in 2D and 3D imaging surveys [36].

Furthermore, the a-spacing and the n-factor (for 2D and 3D cases) are the most important parameters. The main object of these parameters is to select a suitable sequence to achieve real subsurface imaging. These factors are correlated with the DOI and the horizontal coverage of each type of array, signal strength, and sensitivity function to vertical and horizontal change in resistivity [16]. To increase the DOI, the value of n and the value of a is increased. If a large horizontal coverage with a small DOI is required, n has to be decreased and a has to be increased. Furthermore, it is recommended

not to increase n more than 6 times for the DD and WS arrays. Increasing this value more than 6 times decreases the accuracy of the potential measurements and increases the amount of noise [47]. It can also be seen that with increasing n, the levels can be increased for the arrays. These levels refer to horizontal lines of measurements for each value of a; and they are related to the DOI, where the DOI increases with increasing levels. The arrays have many combinations of n and a, according to the desired penetration depth, spatial resolution, and background noise. In general, larger a, and n give relatively deeper information about the geological structure, while small a or small n may offer a relatively good horizontal resolution for the shallower geological sections. As mentioned before, the DD, WN, and WS electrode arrays were applied in this study and these are explained below.

DD array

The arrangement of the electrodes and sensitivity section are explained by Dahlin, Zhou and Loke [8,1]. The distance between potential electrodes (P1-P2) and also between current electrodes (C2-C1) is referred to as a-spacing. However, this array is characterized as well by the n-factor, which describes the distance between the current electrode (C1) and the nearest potential electrode (P1) and is equal to multiples of a-spacing (na). The largest sensitivity values are generally located between C2-C1 and P1-P2 dipole pairs. When the n-factor increases, the high sensitivity values tend to increase beneath the C2-C1 and P1-P2 dipoles while the sensitivity values under the center of the array decrease. In general, the DD array has relatively high anomaly effects and it is more affected by noise than using the WN and WS arrays. This noise might be due to either unusual data or negative readings. The DD array often produces lower signal-to-noise ratios [8]. Moreover, the DD array is much more sensitive to electrode spacing errors than the WN and WS arrays. The electrode spacing error is caused by measurement errors in electrode position or inadvertent electrodes location [48].

However, the geometry of this array plays the most important role in this regard [8]. Therefore, the DD array is not able to determine the horizontal layers due to its bad vertical resolution when depth increases. However, it is suitable to be applied to very shallow investigations. The DD array is highly affected by noise, due to the near-surface inhomogeneity and the lateral subsurface inhomogeneity. Also, the DD array delineates the shallow layers when the distance between its electrodes is small, but it is not capable of recognizing the deeper geological structures when the distance between its electrodes becomes too long (for more information, see [36,44]).

WN array: This array has been more popular as a result of the work carried out by the research group of the Birmingham University [49]. The sensitivity section and the arrangement of the electrodes of this array are explained by [1,8]. There is an almost horizontal contour beneath the center of the array, thus it is relatively sensitive to vertical changes in the subsurface resistivity below the center of the array. However, this array is less sensitive to horizontal changes in subsurface resistivity [1]. Thus it is considered as appropriate to resolve vertical changes but it is poor to some extent to detect horizontal changes.

WS array: This is a new, mixed array lying somewhere between the WN and Schlumberger (SC) arrays [50]. Actually, it is a combination of WN and SC arrays, adapted for using an arrangement with a line of electrodes with a constant spacing, normally used in 2D electrical imaging [51]. However, the normal WN array is a special case of a WS array [51]. Dahlin [8], explained the sensitivity section and electrodes distribution of the WS array. The area of the highest positive sensitivity is below the center of the array. This array is quite sensitive to vertical and horizontal structures [52], so it is useful when vertical and horizontal structures are of interest. Based on the above sequences, the properties for each array used in this study are shown in Table 1.

Array type	Unit ele. Spacing *a* (m)	No. electrodes	n-factor	Max *n* (m)	Max. *a* (m)	Level	Max. DOI	Readings	Time (min)
DD section 1	10	120	1*a*-6*a*	540	90	54	156.1	4671	3:18
DD section 3	10	120	1*a*-6*a*	540	90	54	156.1	4671	3:18
DD section 5	10	120	1*a*-6*a*	540	90	54	156.1	4671	3:18
WS section 1	10	120	1*a*-6*a*	540	90	54	223.2	3240	2:17
WS section 3	10	120	1*a*-6*a*	540	90	54	223.2	3240	2:17
WS section 5	10	120	1*a*-6*a*	540	90	54	223.2	3240	2:17
WN section 1	10	120	*n*=*a*	390	390	39	202.4	2340	1:39
WN section 3	10	120	*n*=*a*	390	390	39	202.4	2340	1:39
WN section 5	10	120	*n*=*a*	390	390	39	202.4	2340	1:39

Table 1: The sequences properties of three conventional electrode arrays, where a: The distance between potential electrodes (P1-P2) or current electrodes (C2-C1), and n: The distance between the current electrode (C1) and the nearest potential electrode (P1).

Results and Discussion

The calculated model is derived from the interpreted model and compared with the field measurements to find the error ratio. The inversion methods try to determine the subsurface model, which corresponds with the field data within acceptable limits [53]. The

inverse models from 2D imaging show three resistivity layers, covering a wide range of resistivity. This resistivity values range from 0.1 Ωm-130 Ωm (Figures 3-5). This wide range of resistivity appears as a consistent pattern in all the inverted models from the three arrays used. The HCB aquiclude clearly appears in all the 2D models as a zone of resistivity between 3 Ωm and 7 Ωm. This HCB is overlain by a layer covering a wide resistivity range of 3 Ωm-130 Ωm.

This layer in turn consists of two resistivity zones. The first zone (3 Ωm-17 Ωm) seems to be partly affected by the movement of the saline water from the KhZ inland. The second zone of the upper layer is interpreted as being a non-affected, upper, unconfined aquifer with resistivity in the range of 20 Ωm-130 Ωm. Below the HCB is a second resistivity layer with the resistivity less than 3 Ωm and most likely represents saline water in the lower aquifer (with TDS of 15,000 mg/L-30,000 mg/L).The 2D inverse models of sections 1 (Figure 3) has three distinct resistivity layers. The first layer consists of two resistivity zones; the first zone has resistivity values in the range of 17 Ωm-130 Ωm, extending to a distance of 450 m. This zone is the upper part of the unconfined aquifer, which consists of pebbles, sand and, clay and it is saturated with brackish groundwater (TDS 5000 mg/L-15,000 mg/L).

The second zone of the first resistivity layer is characterized by resistivity values in the range of 3 Ωm-17 Ωm, and it represents the part of the unconfined aquifer affected by the saline water movement from the KhZ inland. The HCB is recognizable at a depth of 27 m, with a resistivity in the range of 3 Ωm-7 Ωm. The lower aquifer represents the third resistivity layer, which is characterized by saline groundwater with TDS in the range 15,000 mg/L-30,000 mg/L and resistivity of 0.1 Ωm-3.0 Ωm. For lithological correlation, borehole B4 (Figure 4) [27] located far away from the imaging line of 3,000 m has been used.

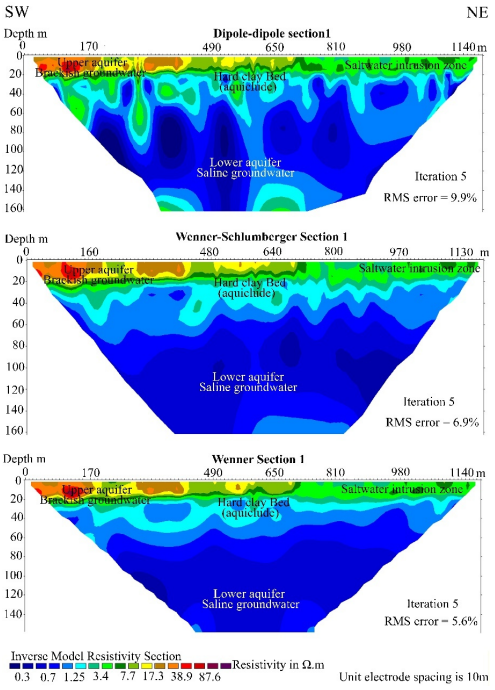

Figure 3: Two-dimensional inverted models of DD section 1, WS section 1 and WN section 1.

To the south of the section 1 (Figure 2) is the 2D inverse models of section 3 (Figure 4) which has the same aforementioned features in its major layers (Figure 3) [27]. The aquiclude HCB appears on this model at a depth of 28 m, having a resistivity of 3 Ωm-7 Ωm. On top of this aquiclude is a layer with two different zones with distinct resistivity values. The first zone starts at the beginning 2D imaging to 270 m (S-W) and has resistivity values between 17 Ωm and 80 Ωm, which represents the upper unconfined aquifer, consisting of clastic sediments, and brackish groundwater (TDS 5000 mg/L-15,000 mg/L).

The second zone of this layer has resistivity values in the range 3 Ωm-17 Ωm and represents an area affected by the saline groundwater extension moving from the KhZ inland. Below the aquiclude is the deep aquifer which is the third major layer, with saline groundwater and TDS of 15,000 mg/L-30,000 mg/L and a resistivity of 0.1 Ωm-2.0 Ωm. For lithological correlation with the inverse models, borehole B9 (Figure 4) [27] located far away from the 2D imaging line of 300 m has been used.

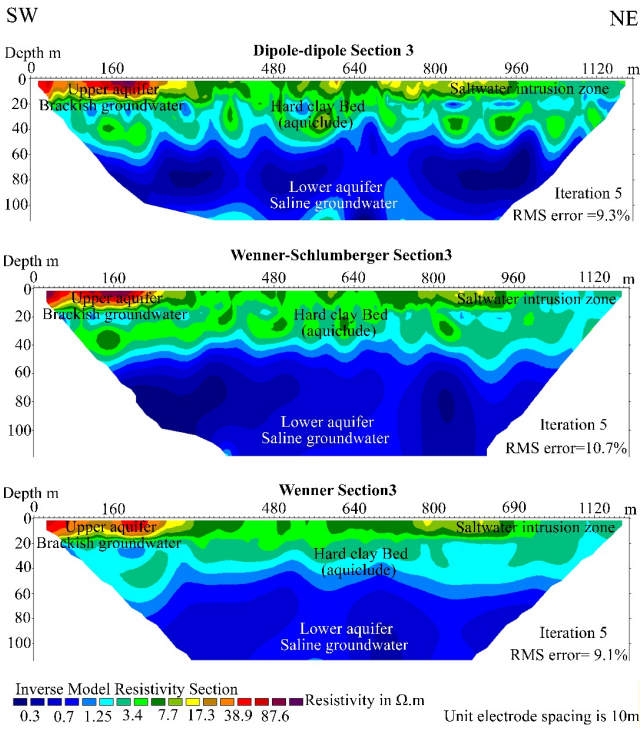

Figure 4: Two-dimensional inverted models of DD section 3, WS section 3 and WN section 3.

To the north of section 1, the 2D inverse models for section 5 (Figure 5) consist of three major layers as well. The first layer has two different zones, the first zone having a resistivity in the range 17 Ωm-70 Ωm, was detected at the beginning 2D imaging to about 160 m. It represents the upper unconfined aquifer consisting of clastic sediments and filled with brackish groundwater. Starting from a distance of 170 m the second resistivity zone appears and extends to the end of section 5. This second zone represents an area affected by the saline groundwater extension moving from the KhZ inland, with a resistivity range of 3 Ωm-17 Ωm. With a resistivity of 1 Ωm-3 Ωm the aquiclude occurs at a depth of 28 m. The lower aquifer is the third major layer characterized by a resistivity of 0.3 Ωm-3.0 Ωm and saline groundwater (TDS 15,000 mg/L-30,000 mg/L). For lithological correlation, boreholes B8 and B11 (Figure 5) [27], has been used.

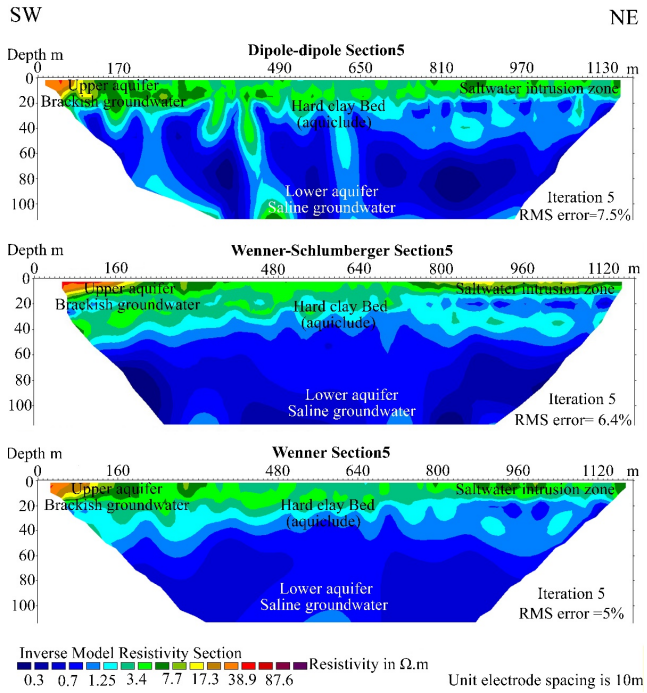

Figure 5: Two-dimensional inverted models of DD section 5, WS section 5 and WN section 5

To compare different types of electrical resistivity arrays, it is important to take into account the shape, boundary, and depth of the investigated target. Emphasizing the reliability of the results is one important criterion. However, this is challenging when the elementary knowledge of the model is limited (in particular, the sharpness or smoothness of the resistivity gradient at the boundaries between different parts of the model). It is worth mentioning that the penetration depth of an array depends mainly on the sensitivity to resistivity contrast, the maximum separation of the electrode array employed in the imaging survey, and the size of the target relative to the burial depth. However, it should be noted that the resolution of the deepest anomalous bodies may be affected by edge effects, due to the reduced data cover for long electrode separation near the end of the electrode layout [1].

In fact, the oblique transition zone between the salt wedge intrusion and the brackish water aquifer is identified and well distinguished in all of the inverted models for the three tested arrays. Nevertheless, the results show some differences, especially in the detection of the HCB (aquiclude) in the subsurface area; a heterogeneous resistive level is presented with a consistent pattern in all the obtained inverse models of all of the arrays used. Moreover, (Figures 3-5) show that the same high variation in the horizontal and vertical resistivity characterize the various inversion models.

Comparison between Arrays

The three arrays used in this study (DD, WN, and WS) were compared with regard to their performance.

DD array

The number of apparent resistivity measurements in the DD array is large compared with the WN and WS array. The DD array was successful in detecting the HCB (aquiclude), better than the WN array but not as accurate as the WS array (in determining the thickness and depth of the HCB (aquiclude); its thickness is overestimated). Moreover, the DD array showed more noise in comparison to the WN and WS arrays. The resolution of the DD array is comparable to that of the WN array, yet it lacks good quality in the case of the WS array nevertheless, the depth resolution of the DD array is not the best when compared with that of the WS and WN arrays. The DD array has better horizontal coverage compared with the WN and WS arrays. Furthermore, the resolution of the DD array inverse models decreases rapidly, although it has large horizontal and vertical coverage data than the WN and WS arrays. When the distance between the electrodes of any array is increased and these electrodes are moved for each measurement, the effect of near-surface and lateral inhomogeneity decrease and vice versa. The DD array is highly affected by near-surface and lateral inhomogeneity in comparison to other arrays. Therefore, the DD array is preferable to be used for cases where rapid horizontal changes in resistivity are expected and shallow investigations are needed.

WS array

The WS array was superior in determining the clay bed (aquiclude) and it gave the greatest depth of investigation in comparison to the DD and WN arrays. The number of measurements was larger than that of the WN array and lower than that of the DD array. It also showed less noise in comparison to the DD and WN arrays. The WS array showed the best inverse models that delineated the upper and lower aquifer and the brackish water/saltwater wedge and display the best resolution with depth. The WS array has a slightly better horizontal coverage compared with the WN array, but it has less horizontal coverage than the DD array. In addition, it has moderate data coverage between the WN and DD arrays. If the distance between the electrodes of any array is increased and these electrodes are moved for each measurement, the effect of near-surface and lateral inhomogeneity will decrease and vice versa. Therefore, the WS array is affected by near-surface and lateral inhomogeneity more than the WN array and less than the DD array. Therefore, the WS array is typically used to determine the sedimentary layers, especially in areas with high background noise and with long survey lines as it gives better results than the DD and WN arrays.

WN array

The WN array is characterized by the lowest number of apparent resistivity measurements among the others; therefore this array fails in providing a good inverse model, even though it is the array least effected by noisy data. Its resolution is still lower than that of the WS array but better than that of the DD array. However, it has a disadvantage in this 2D survey because there is relatively poor horizontal coverage when electrode spacing increases, compared with that of the DD and WS arrays. In the WN array, the a-spacing is the only parameter that controls the measurements. The vertical resolution of the WN array decreases with increasing investigated depth. Thus, its resolution is less than that of the WS for long survey lines and better than that of the DD array. Also, this array was not successful in clearly capturing the horizontal extent of the HCB (aquiclude) and lower aquifer. So, this array is not recommended for deep investigations in the presence of such geological structures.

Figure 6 shows the sensitivity sections for the DD, WS, and WN arrays along section 5. Table 2 also shows the characteristics of each array and it can be seen that the DD array has more data points (3531)

than the others, while the WN has the least (1827). This reflects the higher coverage of the DD array compared with the other arrays. Regarding the number of bad data points, the DD array has 232, the WS array has 149, and the WN is not affected by bad data in the case of section 5. Due to the high number of bad data points, the DD array has the lowest pseudo depth despite the highest coverage, while the WN array has the highest pseudo depth because the status here is reversed. In terms of time, measuring the DD array took longer (195 minutes) than the others in the case of section 5. The WS array took 117 minutes, while the WN array took the shortest time (97 minutes). The WN and WS arrays have the highest number of model blocks (1547) compared with the DD array (1428), therefore, the high sensitivity values in the DD array are in the area beneath the electrodes C1, C2 and P1, P2 but not in the central point of the array. Also, the DD array has the highest average of sensitivity values (8.87) compared with the WS array (4.08) and the WN array (2.12), and this explains why the DD array has the highest number of bad data points and is most affected by poor data. Moreover, the resolution of the WN array is greater near the surface while it decreases with depth, while the DD array possess the lowest resolution and the WS array is the best in this regard; the highest sensitivity values concentrate beneath the center of the array if investigation depth is increased.

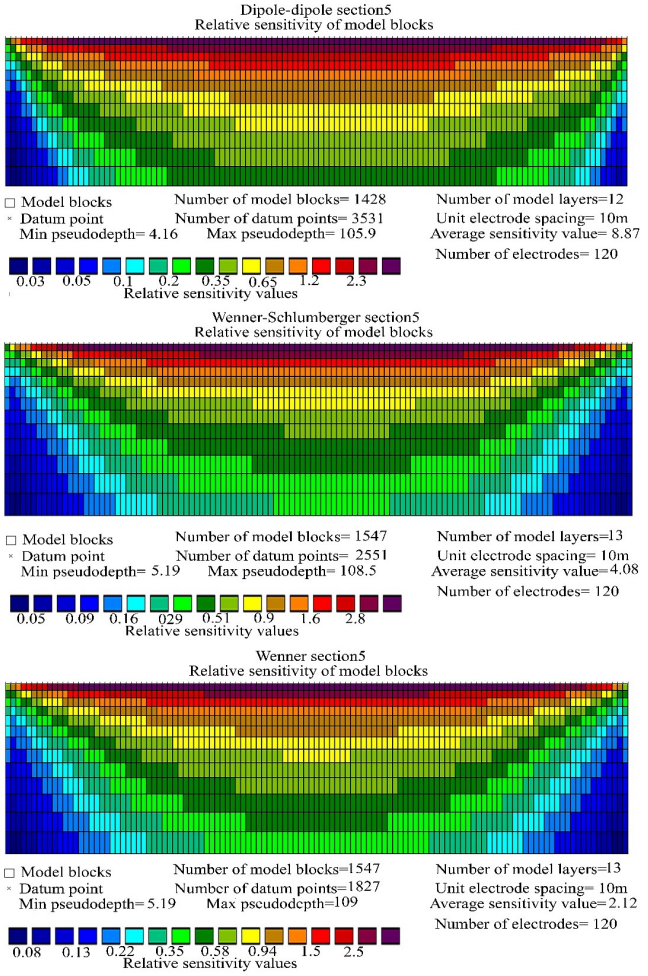

Figure 6: Relative sensitivity sections of arrays-DD section 5, WS section 5, and WN section 5.

Electrode array	Number of model blocks	Number of data	A sensitivity of model blocks	Pseudo depth (m)	Number of bad data	Acquisition time (min)
DD	1428	3531	8.87	105.9	223	195
WS	1547	2551	4.08	108.5	149	117
WN	1547	1827	2.12	109	none	97

Table 2: The properties of sensitivity sections of the DD, WS, and WN arrays along section 5.

Conclusions

Three 2D electrical resistivity configurations, Dipole-dipole, Wenner, and Wenner Schlumberger, were tested in this study in an area in the vicinity to Khor Al-Zubair in southern Iraq. The study area is characterized by horizontal geological layers, with aquifer system consisting of upper unconfined aquifer saturated with brackish groundwater, and lower confined one with saline groundwater, separated by an aquiclude.

All three of the inverse models were able to identify the saline groundwater extension in the uppermost layer and the geological situation but with different horizontal and vertical resolutions. The comparison demonstrated that the Wenner-Schlumberger array was the best in capturing the extension of the anomaly (horizontally and vertically), and it could provide better inverse models which reflected the subsurface lithology. The Wenner-Schlumberger inverse model reflects all hydrogeological and geological features, upper unconfined aquifer, lower confined aquifer, aquiclude, and saline water wedge while the dipole-dipole and Wenner arrays were less precise in determining these features. Moreover, The Wenner-Schlumberger also gave the inverse models with the best resolution, which were least affected by noise, while the results of Wenner and Dipole-dipole were more influenced by noise; therefore, the Wenner and Dipole-dipole arrays could not accurately capture the aquiclude and/or its vertical extension. The Wenner- Schlumberger array gave the most realistic inverse model which coincides with the real situation in the study area. This primarily supports the hypothesis assumed at the beginning of the research.

Acknowledgment

This work was supported by the General Commission for Groundwater of Iraq. The authors would like to express their thanks to Mr. Dhafir Abdullah, Dr. Ahmed Nadhum, and Mr. Abdul Jabbar Hanoon and to the staff of the investigation department for providing all the requirements needed to accomplish this work. Many thanks for Dr. Wael Kanoua for his hints and suggestions.

References

1. Loke MH (2018) Tutorial: 2-D and 3-D electrical imaging surveys. Geotomo Software, Malaysia.
2. Roy A, Apparao A (1971) Depth of investigation in direct current methods. Geophysics 36: 943–959.
3. Koefoed O (1972) Depth of investigation in direct current methods; discussion. Geophysics 37: 703–704.

4. Kearey P, Brooks M, Hill I (2013) An introduction to geophysical exploration. John Wiley & Sons.
5. Telford WM, Geldart LP, Sheriff RE (1990) Applied geophysics. (2nd edition), Cambridge university press.
6. Dahlin T (1996) 2D resistivity surveying for environmental and engineering applications. First Break 14: 275–283.
7. Storz H, Storz W, Jacobs F (2000) Electrical resistivity tomography to investigate geological structures of the earth's upper crust. Geophys Prospect 48: 455–471.
8. Dahlin T, Zhou B (2004) A numerical comparison of 2D resistivity imaging with 10 electrode arrays. Geophys Prospect 52: 379–398.
9. Loke MH, Lane Jr JW (2004) Inversion of data from electrical resistivity imaging surveys in water-covered areas. Explor Geophys 35: 266–271.
10. Loke MH (2010) Res2DInv ver 3.59. 102. Geoelectrical imaging 2D and 3D. Instruction manual. Geotomo Software.
11. Loke MH (2000) Electrical imaging surveys for environmental and engineering studies. A practical guide to 2-D and 3-D surveys.
12. Loke MH (2002) Rapid 2D resistivity forward modeling using the finite difference and finite element methods. Geotomo Software, Malaysia.
13. Park SK, Van GP (1991) Inversion of pole-pole data for 3-D resistivity structure beneath arrays of electrodes. Geophysics 56: 951–960.
14. Van GP, Park SK, Hamilton P (1991) Monitoring leaks from storage ponds using resistivity methods. Geophysics 56: 1267–1270.
15. Sasaki Y (1992) Resolution of resistivity tomography inferred from numerical SIMULATION1. Geophys Prospect 40: 453–463.
16. Zhou W, Beck BF, Adams AL (2002) Effective electrode array in mapping karst hazards in electrical resistivity tomography. Environ Geol 42: 922–928.
17. Hsu H-L, Yanites BJ, Chen C, Chen Y-G (2010) Bedrock detection using 2D electrical resistivity imaging along the Peikang River, central Taiwan. Geomorphology 114: 406–414.
18. Ratnakumari Y, Rai SN, Thiagarajan S, Kumar D (2012) 2 D Electrical resistivity imaging for delineation of deeper aquifers in a part of the Chandrabhaga river basin, Nagpur District, Maharashtra, India. Curr Sci 102: 61–69.
19. Okpoli CC (2013) Application of 2D Electrical Resistivity Tomography in Landfill Site: A Case Study of Iku, Ikare Akoko, Southwestern Nigeria. J Geol Res.
20. Moreira CA, Montenegro Lapola M, Carrara A (2016) Comparative analyzes among electrical resistivity tomography arrays in the characterization of flow structure in free aquifer. Geofísica Int 55: 119–129.
21. Abdelwahab H (2013) Comparison of 2D and 3D resistivity imaging methods in the study of shallow subsurface structures. Greener J Phys Sci 3: 149–158.
22. Thabit JM, Al -- Khersan, Emad H., Abrahem SN (2016) Comparison of 2D Resistivity Imaging Survey Using Wenner, Wenner-Schlumberger and Dipole-dipole Electrode Arrays in Uruk Archaeological Site, Iraq. Almuthanna J Pure Sci 3.
23. AL-Hameedawi MM, Thabit JM (2017) Comparison between four electrode arrays in delineating sedimentary layers of alluvial fan deposits in eastern Iraq using a 2D imaging technique. Environ Earth Sci 76: 525.
24. Thabit JM, Al-Zubedi AS (2015) Evaluation of three important electrode arrays in defining the vertical and horizontal structures in 2D imaging surveys. Iraqi J Sci 56: 1465–1470.
25. Alwan IAK (2013) Comparison between Conventional Arrays in 2D Electrical Resistivity Imaging Technique for Shallow Subsurface Structure Detection of the University of Technology. Eng Technol J 31: 1817–1824.
26. Thabit JM, Abed AM (2013) Evaluation of different electrode arrays in delineation subsurface cavities by using 2D imaging technique. J Univ Anbar Pure Sci 7: 166–175.
27. Abdulameer A, Thabit JM, AL-Menshed FH, Merkel B (2018) Investigation of seawater intrusion in the Dibdibba Aquifer using 2D resistivity imaging in the area between Al-Zubair and Umm Qasr, southern Iraq. Environ Earth Sci 77: 619.
28. Al-Sharbati F, Ma'ala K (1983) Report on the regional geological mapping of west of Zubair area. Iraq-GEOSURV, int rep.
29. Yacoub SY, Purser BH, Al-Hassani NH, et al (1981) Preliminary study of the quaternary sediments of SE Iraq. Jt Res Proj by Geol Surv Iraq Univ Paris XI, Orsay, GEOSURV, Int rep.
30. Water Quality Association Salt Water Definition Review.
31. Al-Kubaisi Q (1999) Quaternary-Tertiary hydrogeologic boundary condition at Safwan-Zubair area. South of Iraq. Iraq Jour Sci 40: 21–28.
32. Manhi H (2012) Groundwater contamination study of the upper part of the Dibdibba aquifer in Safwan area, southern Iraq: Unpublished M. Sc. thesis, University of Baghdad-College of Science P 135. Unpubl M Sc thesis, Univ Baghdad-College Sci P 135.
33. Alkinani M, Merkel B (2017) Hydrochemical and isotopic investigation of groundwater of Al-Batin alluvial fan aquifer, Southern Iraq. Environ Earth Sci 76: 301.
34. Khwedim K, Schneider M, Ameen N, et al (2017) The Dibdibba aquifer system at Safwan--Zubair area, southern Iraq, hydrogeology and environmental situation. Environ Earth Sci 76: 155.
35. Al-Jiburi H, Al-Basrawi N (2009) Geology of Iraqi Southern Desert, Hydrogeology. Iraqi Bull Geol Mining, Spec Pp: 77–91.
36. Loke MH, Barker RD (1995) Least-squares deconvolution of apparent resistivity pseudosections. Geophysics 60: 1682–1690.
37. Loke MH, Barker RD (1996) Rapid least-squares inversion of apparent resistivity pseudosections by a quasi-Newton method. Geophys Prospect 44: 131–152.
38. Yang C-H, Tong L-T, Huang C-F (1999) Combined application of dc and TEM to sea-water intrusion mapping. Geophysics 64: 417–425.
39. Colangelo G, Lapenna V, Loperte A, Perrone A, Telesca L(2008) 2D electrical resistivity tomographies for investigating recent activation landslides in Basilicata Region (Southern Italy). Ann Geophys 51: 1-11.
40. Bernard J (2003) Short note on the depth of investigation of electrical methods. Source: Google search 3: 5.
41. Hiltunen DR, Roth MJS (2004) Investigation of bridge foundation sites in karst terrane via multi-electrode electrical resistivity. Geotech Geophys site Charact Pp: 483–489.

42. Chitea F, Georgescu P (2009) Sensitivity function for various geoelectric arrays.
43. McGillivray PR, Oldenbur g DW (1990) METHODS for calculating fréchet derivatives and sensitivities for the non--linear inverse problem: A comparative study 1. Geophys Prospect 38: 499–524.
44. Edward LS (1977) A modified pseudosection for resistivity and induced-polarization. Geophysics 42: 1020–1036.
45. Barker RD (1989) Depth of investigation of collinear symmetrical four-electrode arrays. Geophysics 54: 1031–1037.
46. Merrick NP (1997) A new resolution index for resistivity electrode arrays. Explor Geophys 28: 106–109.
47. Butler SL (2016) Research Note: The mean sensitivity depth of the electrical resistivity method. Geophys Prospect 64: 1399–1409.
48. Szalai S, Koppán A, Szarka L (2008) Effect of positional inaccuracies on multielectrode results. Acta Geod Geophys Hungarica 43: 33–42.
49. Griffiths DH, Turnbull J (1985) A multi-electrode array for resistivity surveying. First Break 3: 16–20.
50. Pazdirek, O, Blaha V (1996) Examples of resistivity imaging using ME-100 resistivity field acquisition system.
51. Loke MH (2008) RES2DINV version 3.54-Rapid 2D resistivity and IP inversion using the least-squares method: Geoelectrical Imaging 2-D and 3-D. Geotomo Software, Malaysia, 130p.
52. Loke MH (2012) Tutorial: 2D and 3D electrical imaging surveys. Penang, Malaysia, Universiti Sains Malaysia. Unpubl course notes, http//www Geoelectr com.
53. Loke MH, Barker RD (1996) Practical techniques for 3D resistivity surveys and data inversion. Geophys Prospect 44: 499–523.